Continual skipping - getting a kick from water

Ian Hewitt

1   Introduction

Attempting to 'skip' stones at the beach is familiar to many - throwing the stone into the water surface in such a way that it bounces several times before eventually sinking. This project investigates whether, by towing an object along at a sustained horizontal velocity, it can *continually* skip along the surface, and looks at the fluid dynamics which might cause this to happen.

We conduct experiments in which we tow an inclined plane (which we refer to here as a paddle) through the water at different speeds and observe whether it glides steadily through the water or whether it oscillates and skips clear of the surface. We then attempt to explain the observations with some simple models for the height of the paddle.

We find that a light paddle will continually skip provided the water speed is large enough, and the size of the bounces increases with the water speed above this threshhold. We can study how this depends on the mass of the paddle, and also its width.

The steady planing state, at least when treated as two dimensional, is a classical problem [4, 16] and also bears some similarity to steady flow beneath a sluice gate [18, 1] or a surfboard [17]. However the stability of this state has not received much attention and allowing for time dependence significantly alters the problem.

A related body of research looks at 'water entry' of an object, the majority of which has military applications; particularly the impact of torpedoes and bombs on the surface and the forces on a seaplane's floats during landing [19, 20, 8]. The main questions in this case are whether the force exerted by the water on the entering object is large enough to cause it to ricochet off the surface (usually not desired for torpedoes, but famously put to effect by Barnes Willis's 'bouncing bomb'), or whether the seaplane will maintain its stability as a result of the force experienced on the floats.

Mathematical models of the response of both shallow and deep water due to an impacting object have been developed [9, 20, 7], looking at the wetted region of the object, the high speed jets which are ejected and the force on the object; taking into account all the details of the water flow makes the results reasonably complicated. A simpler description of the force on the object was used recently to describe experiments on skipping stones [3, 13], and we use this as a starting point for a description of our experiments. It will be seen that this model is too simplistic and we must add some extra physics - namely the 'splash-up' of water ahead of the object - to explain the observed skipping.
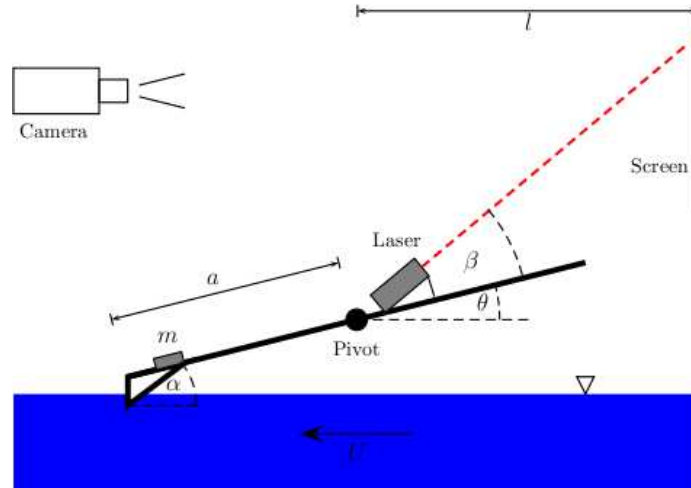
Figure 1: Experimental setup. A counterbalanced wooden arm of length $2a$ is pivoted at a fixed point, with a paddle attached to one end and a laser attached to the other. The paddle side is weighed down by a mass m. The paddle is usually 7 cm wide, although some experiments used a wider 10 cm paddle. The laser shines a beam at an angle β onto a screen where its position is captured by a video camera at 30 frames per second.

2   Experiments

The setup for the experiments is shown in figure 1. We performed most of the experiments in a large (2 m diameter) rotating tank with the paddle held by an arm onto a fixed pivot. By changing the angular velocity of the rotating tank we could adjust the water speed beneath the paddle and arm, which were aligned parallel to the water flow near the edge of the tank.

The arm holding the paddle was counterbalanced on the other side so that the weight of the paddle pulling it down could be made small. By adding additional masses on top of the paddle we could then increase its weight. Attached to the arm was a laser pointer which shined its beam upwards onto a screen (see figure 1). The screen could be recorded with a video camera, and the position of the laser obtained from analysing the images. We used a standard 30 frames per second analog recorder, so could extract the position of the laser every 1/30 of a second. The position of the laser can then be converted into the vertical position of the paddle so that we obtain the trajectory of the paddle sampled at 30 Hz.

The water flowing beneath the paddle was about 6 cm deep, but one of the drawbacks of using a rotating tank was that this depth depended on the flow speed. The surface of the water is not flat - it is parabolic in shape - and becomes more and more inclined as the angular velocity of the tank increases. In order to ensure that the paddle bottom was as near as possible to parallel to the surface (since the surface is parabolic and the paddle straight, this is not possible exactly) the arm holding the pivot had to be angled differently for different water speeds.

The tank could be rotated at up to 2 rad s^{-1}, and the paddle was positioned about 20 cm from the edge of the tank so that the highest possible water speed was 1.76 m s^{-1}.
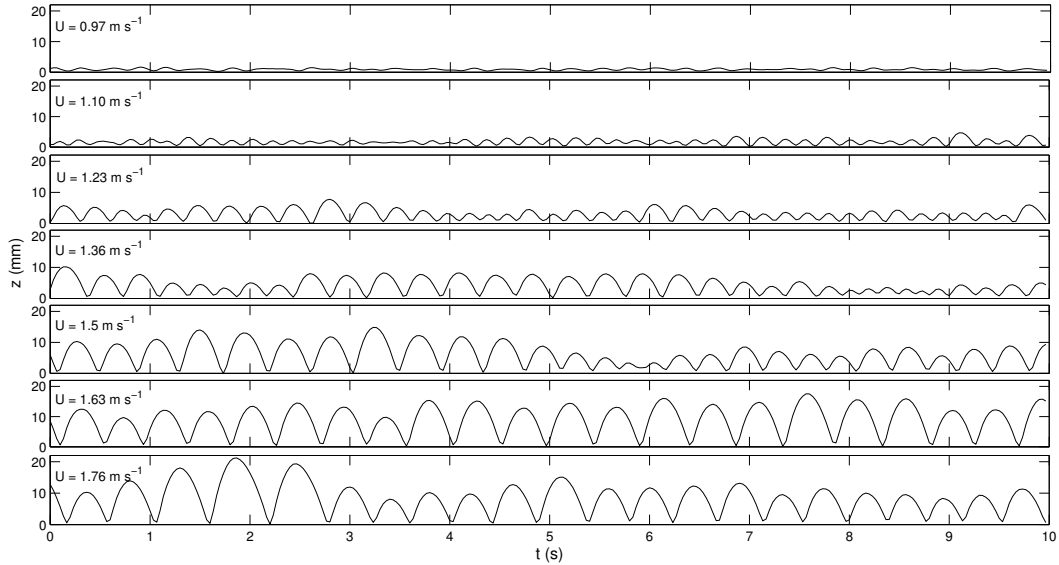
Figure 2: 10 s segments of time series for increasing water speed U and mass $m = 3.4$ g. This is the vertical displacement of the paddle, but the origin in each case is arbitrarily chosen to be the minimum position, and is therefore not quite the same for each speed. The height of the undisturbed water surface is not known exactly but will be between $0 - 5$ mm above the minimum. At lower speeds the paddle sits in a steady planing state without oscillating.

This speed is high enough to cause a light paddle to continually skip along the surface - indeed there seemed to be no steady planing state in this case and independently of how the paddle was dropped or placed into the water it would evolve into a bouncing trajectory which had a characteristic amplitude and frequency. Whilst each bounce was somewhat irregular - they were not all the same amplitude - the amplitude of the bouncing mode over a long enough time series was quite well defined. The trajectory was recorded in 45 second time series which were begun long after the paddle was placed in the water - these trajectories are therefore indicative of the 'steady' bouncing behaviour. Examples of the trajectories obtained are shown in figures 2 and 3. The origin for each of these trajectories is not the same - due to the experimental setup it was not possible to accurately determine where on the screen corresponds to the undisturbed water surface, so the displacements measured can only be regarded as *relative* displacements. It is also not easy to determine when the paddle leaves the water surface - we were only able to assess this visually. It appears that small oscillations are possible with the paddle never leaving the surface - for instance below speed $U = 1.1$ m s^{-1} in figure 2 and above mass $m = 17.3$ g in figure 3.

At high water speeds the rotation period of the tank is only just over 3 seconds, which does not give long for the waves created in the wake of the paddle to be carried round into its path. We would like the water ahead of the paddle to be as smooth as possible, since we are looking for natural oscillations rather than setting up a wave pattern around the tank (unlike [15], for example), so ideally we would like to remove the wake entirely. This
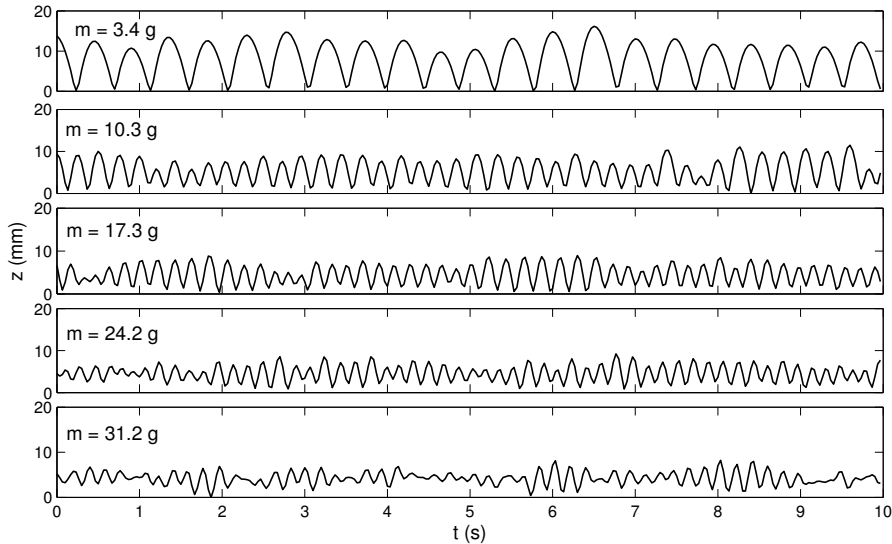
Figure 3: 10 s segments of time series for 5 different masses, with water speed $U = 1.5 \text{ m s}^{-1}$. This is the vertical displacement of the paddle, but the origin in each case is arbitrarily chosen to be the minimum position, and is therefore not quite the same for each mass. The height of the undisturbed water surface is not known exactly but will be around 5 mm above the minimum.

is another drawback of the rotating tank setup, and we attempted to minimise the wave activity ahead of the paddle by padding the sides of the tank with netting, to damp the waves which reflect off the walls. At large water speeds the center of the tank was also dry so we similarly padded the inner 'shoreline' where the waves would otherwise break and reflect. This had some effect in smoothing out the water, though we cannot claim to have removed the waves entirely. However, we do not believe that the presence of waves ahead of the paddle is what causes the oscillations - although it may lead to a more noisy signal than we could expect if the water surface were really smooth. By dropping the paddle into smooth water it was observed that the regular amplitude of bounces was set up *before* the first wake had travelled round the tank, suggesting that excitation by the waves is not the driving mechanism.

The main parameters we varied were the speed of the water U and the mass on the paddle m, as shown in figures 2 and 3. The power spectrum of these trajectories has a peak at frequencies close to the evident natural frequency of oscillations, but it is not very well defined, and the amplitude of the peak is not a good measure of the amplitude of oscillations. This might be expected since when the paddle leaves the water it ought to follow a parabolic ballistic trajectory, whereas in the water it may be more sinusoidal; the combination cannot be expected to decompose clearly in Fourier coefficients.

Instead we analyse the data by isolating individual bounces or oscillations and calculating their amplitude and period. Each 45 second time series contains over 100 bounces so we can look at the mean and standard deviation; these are shown in figures 4 and 5. The standard deviation gives a measure of how variable the amplitude and period are and there-
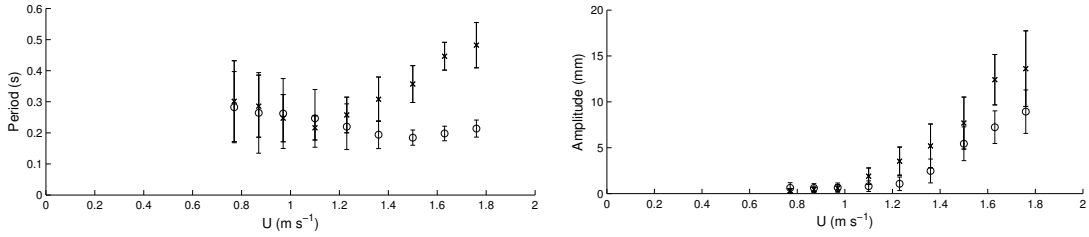
Figure 4: Period and amplitude for a paddle of mass 3.4 g (crosses) and mass 17.3 g (circles), with different water speeds U. These are average periods and amplitudes of oscillations over a 45 s time interval. The error bars are one standard deviation either side of the mean, and therefore give an indication of the variability rather than the error.
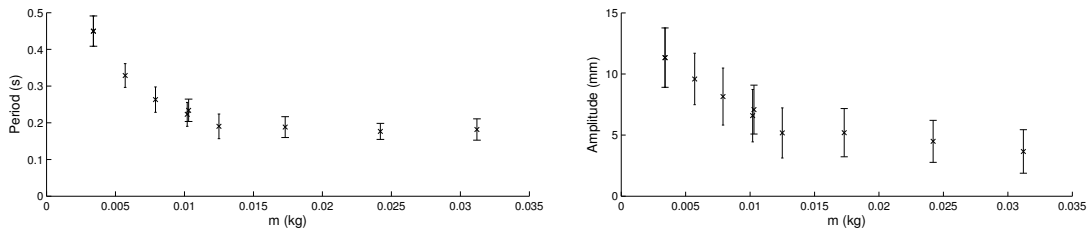

Figure 5: Period and amplitude for water speed $U = 1.5 \text{ m s}^{-1}$, with different paddle masses m. This shows the average period of oscillation and amplitude, with the error bars showing one standard deviation either side of the mean. These are taken from the amplitudes and periods of bounces within a 45 s time interval.

fore how well defined the bouncing mode is. At slow speeds, the trajectories are seen to be considerably more noisy and irregular and this is evident in the larger standard deviation for the period.

To summarise what these data show, for a given paddle mass there seems to be a threshold water speed above which oscillations start to occur (figure 4), and above this, the amplitude of the oscillations increases, apparently linearly, with the water speed. This is suggestive of some sort of bifurcation, and we also see that the threshold seems to be higher for a heavier paddle. When the bounces have large amplitude, there is a simultaneous increase in the period, as we might expect for ballistic trajectories.

For a constant water speed (figure 3), it appears that the lighter mass undergoes larger oscillations with a longer period and as the mass is increased the amplitude and period decrease, with the period levelling off towards a roughly constant 0.2 s.

These are some of the trends which we hope to be able to explain, at least qualitatively, with a simple model.

We also conducted some experiments with a wider paddle of width 10 cm to examine the effect of the paddle's width. For the same mass, the wider paddle undergoes larger amplitude bounces and appears to require a lower threshold water speed to start oscillating (figures 6 and 7). This dependence on the width of the paddle is another feature which we
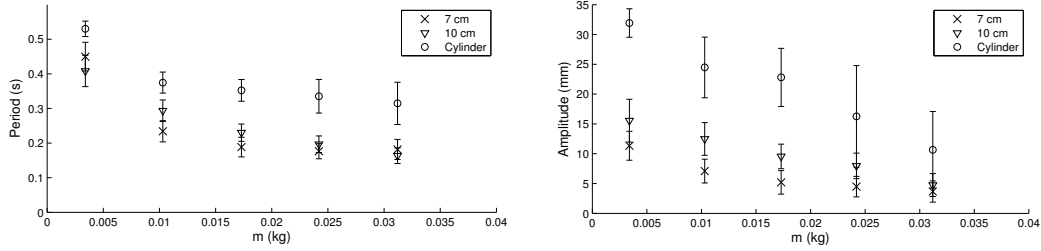
Figure 6: Period and amplitude for water speed 3.5 m s^{-1}, for 5 different masses with 7 cm and 10 cm wide paddles and with a cylinder shaped paddle. These are average periods and amplitudes of oscillations over a 45 s time interval. The error bars are one standard deviation either side of the mean.
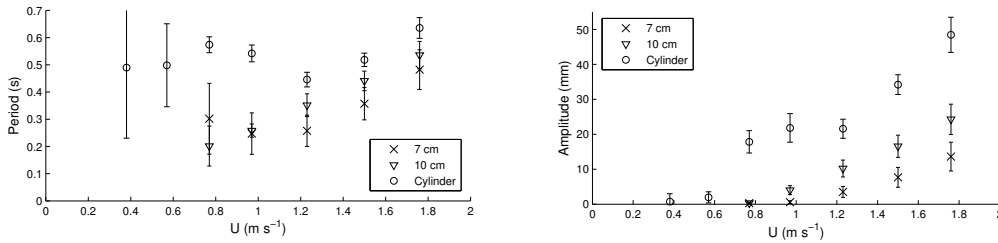

Figure 7: Period and amplitude for a paddle of mass 3.4 g for different water speeds with 7 cm and 10 cm wide paddles and with a cylinder shaped paddle. These are average periods and amplitudes of oscillations over a 45 s time interval. The error bars are one standard deviation either side of the mean.

hope the model will capture.

Though we will not discuss them further we also did some tests with a cylindrical paddle (lengthways across the stream). This oscillated very regularly and with large amplitude and the threshold to begin oscillating was at a considerably lower water speed. The data are shown in figures 6 and 7 for completeness.

3 Modeling preliminaries

The vertical position of the paddle is governed by the angle θ between the arm and the horizontal, so the equation of motion is really conservation of angular momentum about the pivot. The equation is

$$\mathcal{I}\ddot{\theta} = -mga\cos\theta + Fa\cos\theta - \mu a^2\dot{\theta}, \tag{1}$$

in which $\mathcal{I}$ is the moment of inertia, a is the length of the arm, m is the excess weight on the paddle side, g is the gravitational acceleration, and F is the vertical force of the water on the paddle. μ is a friction coefficient which describes the damping by friction in the hinge and air resistance. The vertical displacement of the paddle is $z = a\sin\theta$ and since θ
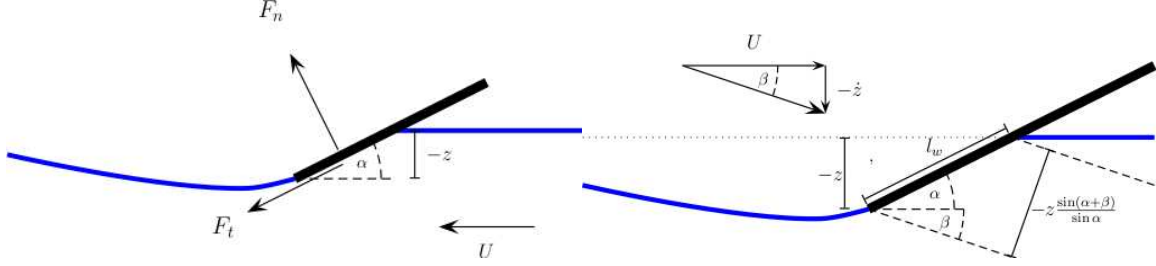
Figure 8: (a) Forces on a paddle inclined at an angle α to the horizontal water surface, in a stream moving at speed U. z, measured vertically upwards, is the position of the paddle tip above the undisturbed surface. (b) Geometry of paddle in the frame of the moving water. The wetted length l_w shown here is the length of the paddle beneath the undisturbed free surface.

is small we can approximate the equation as

$$(M + m)\ddot{z} = -mg + F - \mu\dot{z}, \tag{2}$$

in which we define the effective mass M by $\mathcal{I} = (M + m)a^2$.

The Reynolds number based on the depth of the water is large, and is still large even if the length scale is taken as the depth of the paddle (~ 5 mm),

$$Re = \frac{UH}{\nu} \sim 10^4 - 10^5. \tag{3}$$

The relevance of surface tension is seen from the Weber number

$$We = \frac{\rho U^2 z}{\sigma} \sim 100, \tag{4}$$

in which we take z to be a typical depth of the paddle. Since this is large, inertia is much more important than surface tension forces which we will henceforth discount.

The remaining forces from the water might be separately described as buoyancy (hydrostatic pressure), hydrodynamic pressure and hydraulic drag. The buoyancy is simply the weight of the water displaced by the wedge shape of the paddle $\rho g W z^2 / 2 \tan \alpha$, which we will see is negligible in comparison with the hydrodynamic force $\rho U^2 W z$ at the speeds ($U \sim 1$ m s^{-1}) of interest. The Froude number U^2/zg is large, and this is indicative of the fact that buoyancy is not the principal force from the water; for simplicity, we will therefore neglect any effects of gravity on the water.

The vertical force of the water on the paddle can therefore be written as

$$F = F_n \cos \alpha - F_t \sin \alpha \tag{5}$$

where F_n is the force acting in the normal direction on the paddle and F_t is the force acting in the downwards tangential direction. We expect the normal force here to be due to the hydrodynamic pressure and the tangential force to be due to hydraulic drag, and for the purposes of the current experiment we expect the normal force producing *hydrodynamic lift* to be the most important.

We begin by following the approach used with some success to model skipping stones [2, 3, 13], in which the force depends on the relative velocity of the stone or paddle, and its depth in the water. At high Reynolds number, such a force takes the form

$$F = \frac{1}{2}C\rho|\mathbf{U}|^2 A, \tag{6}$$

in which $\mathbf{U} = -U\mathbf{i} + \dot{z}\mathbf{k}$ is the relative velocity, A is the cross sectional area of the object, and C is a coefficient.

For the context of an object entering the water we expect that the relevant area should be the cross sectional area in the direction of motion. For an object traveling at an angle $\beta = -\tan^{-1}(\dot{z}/U)$ to the horizontal (relative to stationary water) we can therefore expect (figure 8),

$$F_n = \frac{1}{2}\rho|\mathbf{U}|^2 A = \frac{1}{2}\rho|\mathbf{U}|^2 W l_w \sin(\alpha + \beta), \tag{7}$$

where $l_w = -z/\sin\alpha$ is the 'wetted length' of the paddle, and W is the width of the paddle. Note that the wetted length here is taken as being the length of the paddle beneath the undisturbed water surface: this definition will need to be refined later. This expression for the force was deduced from experiments conducted by Rosellini et al. [13], but can be understood in terms of the geometry of figure 8. The coefficient C in (6) is therefore 1 in this case, provided we choose the correct definition of the area A.

(7) can be written as

$$F_n = -\frac{1}{2}\rho W (U^2 + \dot{z}^2)^{1/2} z(U - \cot\alpha \ \dot{z}), \tag{8}$$

and when $\dot{z}$ is much smaller than U (an approximation which is appropriate for our experiment) this force becomes linear in z and we have, ignoring friction for the moment,

$$(M + m)\ddot{z} = -mg - \frac{1}{2}\rho W \cos\alpha \ U^2 z, \tag{9}$$

This is a linear spring equation which oscillates about the steady position

$$z_0 = -\frac{2mg}{\rho W \cos\alpha \ U^2}, \tag{10}$$

with frequency

$$\omega = \left[\frac{\rho W \cos\alpha \ U^2}{2(M + m)}\right]^{1/2} \text{rad s}^{-1}. \tag{11}$$

However this assumes that the paddle is always in the water, whereas of course if it goes above the surface it no longer feels the effect of the water at all. So we can write the equation of motion as

$$\ddot{z} = \omega^2 z_0 - \omega^2 z \mathcal{H}(-z), \tag{12}$$

where $\mathcal{H}(-z)$ is the Heaviside function (0 for $z > 0$ and 1 for $z < 0$). If the oscillations have large enough amplitude they will go above the surface and have projectile motion in the air,
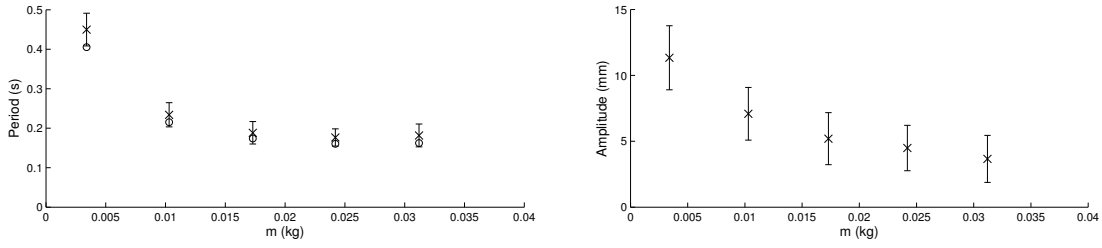
$$\ddot{z} = \omega^2 z_0. \tag{13}$$

281

Figure 9: Average period and amplitude of oscillations over a 45 s time interval, for water speed $U = 1.5$ m s^{-1}, with 5 different masses. The error bars show one standard deviation either side of the mean (crosses), and the circles show the theoretical prediction for the period (17) if the amplitude is fitted to the observed average for each mass.

Figure 10: Average period and amplitude of oscillations over a 45 s time interval, for paddle mass $m = 3.4$ g, with different water speeds. The error bars show one standard deviation either side of the mean (crosses), and the circles show the theoretical prediction for the period (17) if the amplitude is fitted to the observed average for each speed.
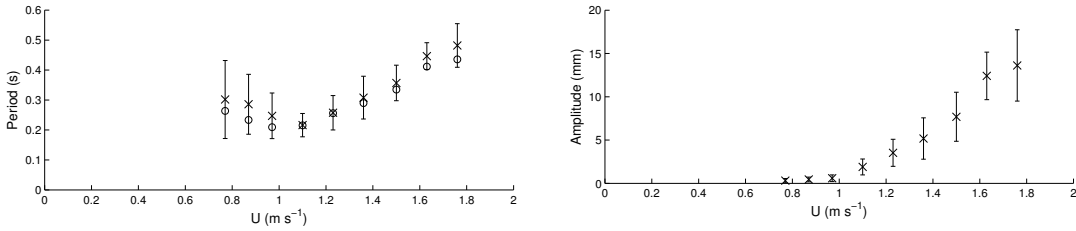
The velocity is zero at the maximum height H, and the path is parabolic,

$$z = H + \frac{1}{2}\omega^2 z_0 t^2, \tag{14}$$

entering the water at time $t_c = (-2H/\omega^2 z_0)^{1/2}$ with velocity $v = -(-2H\omega^2 z_0)^{1/2}$. After this the motion is sinusoidal

$$z = z_0 - z_0 \cos\omega(t - t_c) - (-2Hz_0)^{1/2}\sin\omega(t - t_c), \tag{15}$$

and will exit the water again at a time

$$t = t_c + \frac{2}{\omega}\left[\pi - \tan^{-1}\left(-\frac{2H}{z_0}\right)^{1/2}\right]. \tag{16}$$

The period of the whole oscillation (for $H > 0$) is therefore

$$\frac{2}{\omega}\left[\pi - \tan^{-1}\left(-\frac{2H}{z_0}\right)^{1/2} + \left(-\frac{2H}{z_0}\right)^{1/2}\right]. \tag{17}$$

282

Unlike a simple harmonic oscillator the frequency now depends on the amplitude of the motion, which is seen from the solutions to be

$$H - z_0 + (z_0^2 - 2Hz_0)^{1/2}. \tag{18}$$

Thus, if we know the amplitude of oscillations we should be able to predict the period or frequency. By taking the observed amplitudes of the oscillations in the experiment we can estimate what the periods should be, and the results of such calculations are shown in figures 9 and 10.

However, there is nothing in (12) which sets the amplitude of oscillations - they are purely determined by the initial conditions. Moreover, if we introduce the frictional term $-\mu\dot{z}$ any initial conditions will eventually decay towards the steady state. The same will be true for any force $F(z)$, since the change in energy over a collision starting with $z = 0$ at $t = t_{IN}$ and ending at $z = 0$ at $t = t_{OUT}$ is

$$\left[\frac{1}{2}(M + m)\dot{z}^2\right]_{t_{IN}}^{t_{OUT}} = \int_{t_{IN}}^{t_{OUT}} -mg\ \dot{z}\ \mathrm{d}t + \int_{t_{IN}}^{t_{OUT}} F_n(z)\cos\alpha\ \dot{z}\ \mathrm{d}t - \int_{t_{IN}}^{t_{OUT}} \mu\dot{z}^2\ \mathrm{d}z \tag{19}$$

$$= -\int_{t_{IN}}^{t_{OUT}} \mu\dot{z}^2\ \mathrm{d}z < 0. \tag{20}$$

Thus any force which is a function only of z will result in damped oscillations. In the experiments we observe that there are oscillations which continue indefinitely, and their amplitude naturally selects itself. Thus in the equation of motion (2) there must be some destabilzing process which drives oscillations and it is then the balance between this and the stabilizing effects of friction which determines their amplitude.

We see that approximating the force in (8) by the linear force in (9) cannot explain the observed oscillations. By including the full force (8) we also find that the additional nonlinear terms have a dissipative effect; figure 11 shows the solution to the equation of motion with F taken as the vertical component of (8):

$$(M + m)\ddot{z} = -mg - \frac{1}{2}\rho W\cos\alpha(U^2 + \dot{z}^2)^{1/2}z(U - \cot\alpha\ \dot{z}). \tag{21}$$

For comparison the solution is compared with the solution when the horizontal velocity $U = \dot{x}$ is also allowed to vary due to the horizontal component of (8),

$$(M + m)\ddot{x} = -\frac{1}{2}\rho W\sin\alpha(U^2 + \dot{z}^2)^{1/2}z(U - \cot\alpha\ \dot{z}), \tag{22}$$

as is appropriate for the usual case of a skipping stone.

It seems that the force in (8) is inadequate to describe our observations because it does not contain any destabilizing effect. This is more evident in the experiments if we look at the vertical velocity of the paddle while it is continually skipping. Figure 12 shows this velocity alongside the displacement of the paddle, and it is seen that the vertical velocity is on average larger when it leaves the water than when it enters the water. Plotting the exit velocity against entry velocity for each collision (figure 13) we find that the collisions are super-elastic, meaning the coefficient of normal restitution $e = V_{OUT}/V_{IN}$ is larger than 1, and this effect grows as the speed of the water is increased.
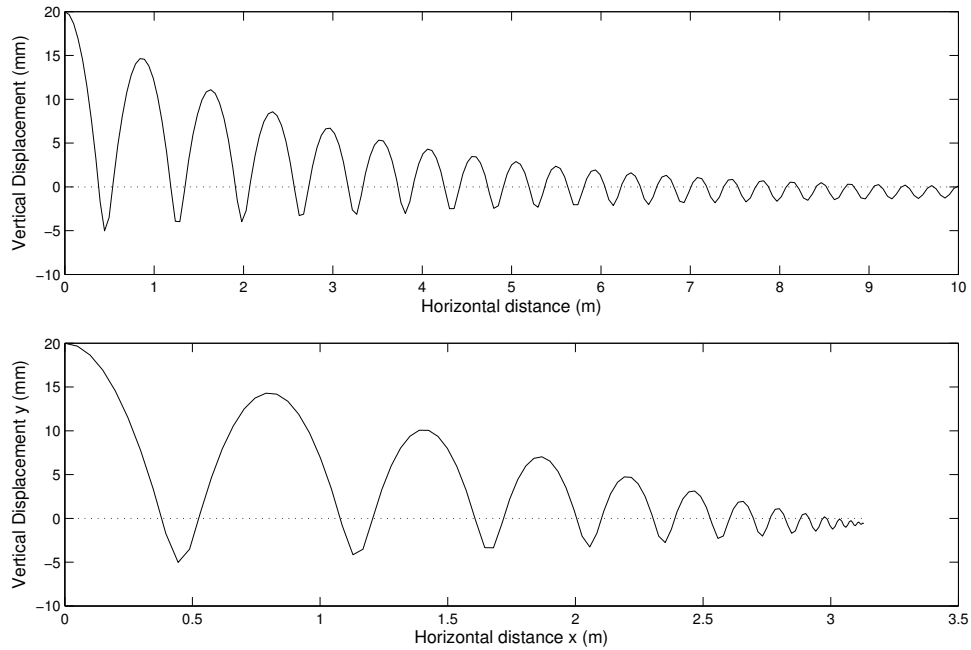
Figure 11: (a) Trajectory of a light stone skipping using Rosellini et al.'s [13] parameterisation of the hydrodynamic force on the stone, with the horizontal velocity imposed as $U = 1.5$ m s^{-1} (21). In this case the distance x is equivalent to time t. The dashed line shows the undisturbed water level. The vertical force on the particle varies through the collision, causing the bounces to decay. (b) The same but with the horizontal velocity unconstrained, so that the position $x(t)$ is determined from (22). The horizontal velocity starts at 1.5 m s^{-1} and decreases to zero due to the force of the water.
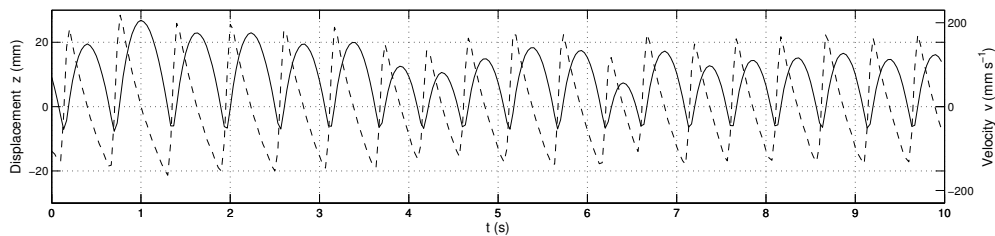

Figure 12: Vertical displacement (solid, left axis) and vertical velocity (dashed, right axis), for the 10 cm wide paddle with mass 3.4 g and water speed $U = 1.76$ m s^{-1}.
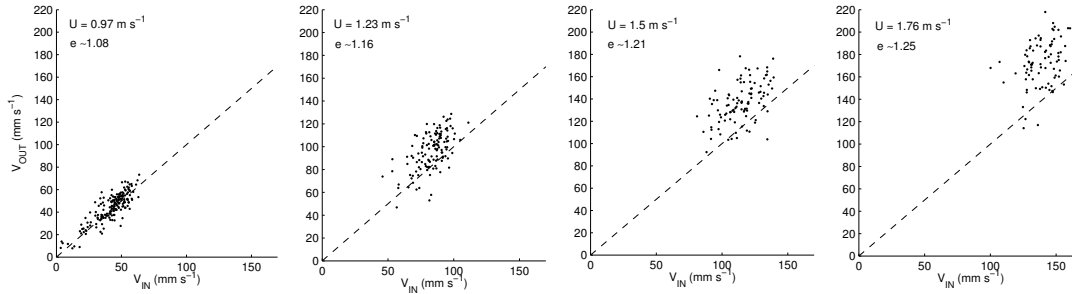
Figure 13: Maximum downward velocity (V_{IN}) plotted against the immediately following maximum upward velocity (V_{OUT}) for each oscillation in a 45 second time interval, for the 10 cm wide paddle with mass 3.4 g and different water speeds U as shown. V_{IN} and V_{OUT} presumably occur somewhere close to where the paddle enters the water when it is bouncing. The values given for the effective coefficient of restitution e are the average of V_{OUT}/V_{IN}.

So the paddle gains kinetic energy during collisions, and this kinetic energy gain must be balanced by the loss due to friction during the air-borne motion. In the next section we discuss what aspects of the hydrodynamic force that can cause this are missing from (8).

3.1   The rise of water ahead of the paddle

The discussion of the previous section leads us to believe that the force from the water cannot be simply a function of the depth beneath the undisturbed surface level, but varies in a more complicated way throughout the course of the collision. The reason for this is due to the water ahead of the paddle piling up there, so that the effective depth, and therefore the wetted length l_w are not just dependent on z (figure 14). This fact was realised by Wagner [20] who noted that the water around an impacting object rises up to meet it, so that the area of the water wetting the object is like an expanding plate. Thus the region over which the water pressure is appreciable is not simply the region beneath the undisturbed surface, but a larger region. It is necessary to determine what this region is and how it varies during the course of the collision in order to calculate the force on the object.

A similar mechanism has been used to explain anomalous (larger than 1) values of the coefficient of normal restitution in oblique elastic collisions - the surface deforms asymmetrically so that the effective normal for the collision is tilted [11, 10].

We can still think of the force as in (7), but we need to take more care in determining l_w. There have been some experimental studies of the water rise ahead of a planing hull [12] which attempt to determine the wetted length as a function of the hull's width and trim angle (α). However we expect the *variation* of this wetted length to be important and in particular we need to consider how l_w varies during the course of the collision. It is not entirely clear how to do this in a simple way, so we begin by considering a two-dimensional shallow water model.

285

Figure 14: Snapshots of paddle and free surface over the course of a collision showing the evolution of the splash-up region ahead of the paddle.
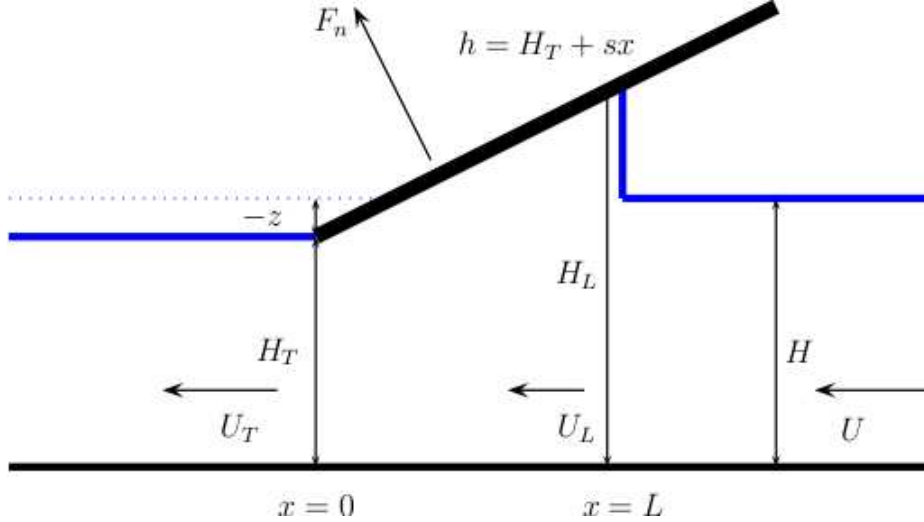

Figure 15: Shallow water model setup with the definition of the water depths H, H_L and H_T, and the position of the shock $x = L(t)$. The upstream conditions H, U are prescribed constants, but the other variables are changing over the course of the collision.

4 Shallow water model

The situation we consider is shown in figure 15; it is similar to the steady case modeled by Tuck & Dixon [17, 14] for the shallow flow beneath a surfboard. The difference between their model and ours is that we allow the height of the paddle to change and we treat the jet which is ejected ahead of the paddle as producing a leading 'wedge' of water. We treat this splash-up region ahead of the paddle as a shock, similar to a tidal bore on a river estuary. The shallow water equations that apply beneath the paddle are, neglecting gravity,

$$h_t - (uh)_x = 0, \tag{23}$$

$$\bar{\rho}(u_t - uu_x) = p_x, \tag{24}$$

in which h is the water depth, u is the velocity in the negative x direction, p is the pressure and $\bar{\rho} = \rho W$ is the two-dimensional density.

The upstream values H and U are steady, and the values at the trailing edge are labeled $h = H_T$ and $u = U_T$ (these will vary in time). At the shock $x = L(t)$ we label $h = H_L$ and $u = U_L$; the differential equations (23) and (24) don't apply here since there is a discontinuity, but mass and momentum must still be conserved so we require jump

286

conditions,

$$-(\bar{\rho}H_L - \bar{\rho}H)\dot{L} = (\bar{\rho}H_L U_L - \bar{\rho}HU), \tag{25}$$

$$-(\bar{\rho}H_L U_L - \bar{\rho}HU)\dot{L} = (\bar{\rho}H_L U_L^2 + p_L H_L - \bar{\rho}HU^2). \tag{26}$$

Note that the pressure on the upstream face of the shock is zero (atmospheric), since we are neglecting gravity.

If we know the position of the trailing edge of the paddle z above the undisturbed surface then $H_T = H + z$ and the depth of water beneath the paddle (for $0 < x < L(t)$) is

$$h(x,t) = H_T + sx, \tag{27}$$

where $s = \tan\alpha$ is the slope of the paddle.

The velocity $u(x,t)$ under the paddle is therefore related to the velocity at the trailing edge by mass conservation (23),

$$u(x,t) = \frac{u_T H_T + \dot{z}x}{H_T + sx} = U + \frac{(H+z)\Delta U - (sU - \dot{z})x}{H + sx + z}, \tag{28}$$

in which we define $\Delta U = U_T - U$ as the change in water speed from upstream to downstream of the paddle. The pressure is obtained from integrating the momentum equation (24), also in terms of ΔU;

$$\frac{p(x,t)}{\bar{\rho}} = \frac{(sU + s\Delta U - \dot{z})^2 x}{s(H + sx + z)} - \frac{(sU + s\Delta U - \dot{z})^2 x^2}{2(H + sx + z)^2} + \frac{\ddot{z}x}{s}$$
$$+ \frac{(H+z)(s\Delta\dot{U} - \ddot{z}) + \dot{z}(sU + s\Delta U - \dot{z})}{s^2}\log\left(1 + \frac{sx}{H+z}\right), \tag{29}$$

the dots all denoting time derivatives.

Combining the jump conditions (25) and (26) gives

$$p_L(H_L - H) = \bar{\rho}H(U - U_L)^2, \tag{30}$$

in which we know

$$H_L = H + z + sL. \tag{31}$$

(25) and (30), with H_L, u_L and p_L coming from (31), (28) and (29), give two equations for the unknowns L and ΔU which also involve z and its time derivatives, and must therefore be coupled with the equation of motion for the paddle

$$(M + m)\ddot{z} = -mg + F_n\cos\alpha - \mu\dot{z}, \tag{32}$$

with F_n now given by

$$\frac{F_n(t)}{\bar{\rho}} = \int_0^{L(t)} \frac{p(x,t)}{\bar{\rho}}\,\mathrm{d}x = \frac{(sU + s\Delta U - \dot{z})^2 L^2}{2s(H + sL + z)} + \frac{\ddot{z}L^2}{2s}$$
$$+ \left((H+z)(s\Delta\dot{U} - \ddot{z}) + \dot{z}(sU + s\Delta U - \dot{z})\right)\left\{\frac{H + sL + z}{s^3}\log\left(1 + \frac{sL}{H+z}\right) - \frac{L}{s^2}\right\}, \tag{33}$$

The combination (25), (30), (31), (28), (29), (32) and (33) provides 3 ordinary differential equations for the unknowns z, L and ΔU. The initial conditions for the start of a collision are

$$z = 0, \quad \dot{z} = V_{IN}, \quad L = 0, \quad \Delta U = 0, \qquad \text{at} \quad t = 0. \tag{34}$$

(29) provides an expression for p_L, and from (30) we also have

$$\frac{p_L}{\bar{\rho}} = \frac{H\big((H+z)\Delta U - (sU - \dot{z})L\big)^2}{(H + sL + z)^2(sL + z)}. \tag{35}$$

Combining these we get an expression for $\Delta\dot{U}$,

$$\Delta\dot{U}\frac{H+z}{s}\log\left(1 + \frac{sL}{H+z}\right)$$
$$= \frac{H\big((H+z)\Delta U - (sU - \dot{z})L\big)^2}{(H + sL + z)^2(sL + z)} - \frac{(sU + s\Delta U - \dot{z})^2 L}{s(H + sL + z)} + \frac{(sU + s\Delta U - \dot{z})^2 L^2}{2(H + sL + z)^2}$$
$$- \frac{\dot{z}(sU + s\Delta U - \dot{z})}{s^2}\log\left(1 + \frac{sL}{H+z}\right) - \frac{\ddot{z}}{s^2}\left(sL - (H+z)\log\left(1 + \frac{sL}{H+z}\right)\right), \tag{36}$$

which can be substituted into the force (33) in the equation of motion to find $\ddot{z}$. After rearrangement we obtain

$$\ddot{z}\left[\frac{M+m}{\rho W\cos\alpha} - \frac{L^2}{2s} + \frac{(H+sL+z)L\log\left(1 + \frac{sL}{H+z}\right) - sL^2}{s^2\log\left(1 + \frac{sL}{H+z}\right)}\right]$$
$$= -\frac{mg}{\rho W\cos\alpha} - \frac{\mu}{\rho W\cos\alpha}\dot{z} + \frac{(sU + s\Delta U - \dot{z})^2 L^2}{2s(H+sL+z)} + \frac{(H+sL+z)\log\left(1 + \frac{sL}{H+z}\right) - sL}{s\log\left(1 + \frac{sL}{H+z}\right)}$$
$$\times\left[\frac{H\big((H+z)\Delta U - (sU - \dot{z})L\big)^2}{(H+sL+z)^2(sL+z)} - \frac{(sU + s\Delta U - \dot{z})^2 L}{s(H+sL+z)} + \frac{(sU + s\Delta U - \dot{z})^2 L^2}{2(H+sL+z)^2}\right]. \tag{37}$$

We are left with the substantially shorter equation for $\dot{L}$,

$$(sL + z)\dot{L} = -H\Delta U - (U + \Delta U)z - \dot{z}L. \tag{38}$$

These equations apply only when the paddle is in the water; that is, $L > 0$. When $L < 0$, the paddle follows a ballistic trajectory given by

$$(M + m)\ddot{z} = -mg - \mu\dot{z}. \tag{39}$$

The equations (36), (37) and (38) must be solved numerically, and a typcial solution is shown in figure 16. Potential singularities in the equations are avoided by switching to equation (39) whenever L is smaller than some small threshold.

It is found that the long term behaviour is independent of the initial condition - at very low water speeds there is a steady state which is stable, but at higher water speeds there is a natural amplitude oscillatory mode, towards which any initial condition will evolve.
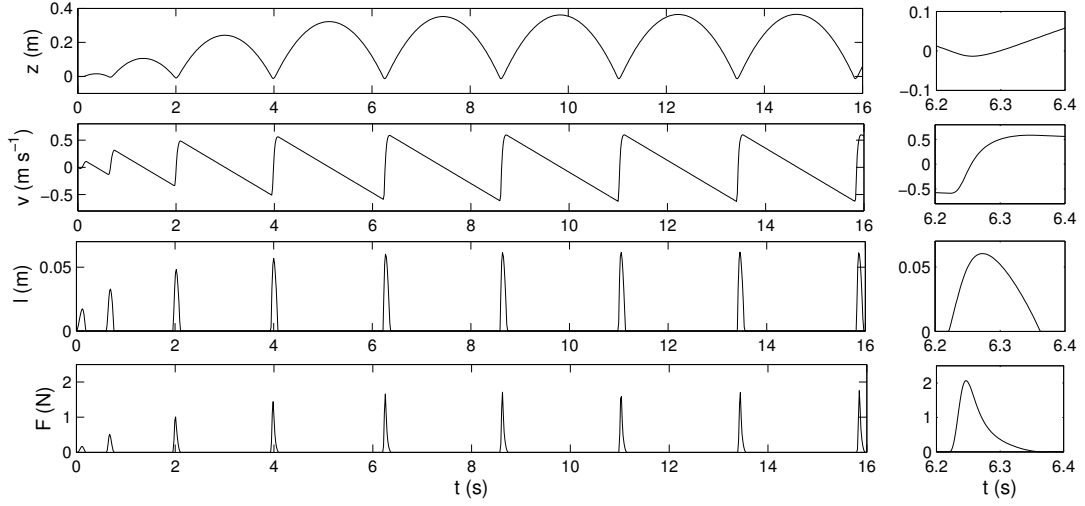
Figure 16: Solution to the shallow water model, (36), (37) and (38) with no friction or mass loss terms, showing the vertical position z, velocity $v = \dot{z}$, position of shock L and vertical force F. The depth is 6 cm, the water speed is 1.5 m s^{-1}, and the paddle mass is 3.4 g. The initial condition is to start from rest on the undisturbed surface $z = 0$. On the right is an enlarged view of one of the collisions.

4.1 Flow around the sides of the paddle

It is evident from figure 16 that these oscillations are considerably larger than those observed in the experiment, with a consistently longer period. One reason for this is undoubtedly the fact that the current model is two dimensional and the water is forced to flow under the paddle, whereas what actually happens is that a substantial fraction of the water passes around the paddle to the sides.

One way of including this mass loss into the two dimensional model is to treat it as occurring at the shock front, so that instead of conserving mass the shock actually allows a certain amount to be lost. If the position of the shock is $x = L$, then the area of the triangular wedge which has built up ahead of the paddle is $sL^2/2$. We might expect on dimensional grounds that the rate at which mass is lost to the sides is proportional to this area and the speed of the water, so that the mass loss is

$$-\lambda \rho s L^2 U. \tag{40}$$

Then the modified jump condition (25) becomes

$$-\rho W (H_L - H)\dot{L} = \rho W (H_L U_L - HU) + \rho s L^2 U. \tag{41}$$

With this modification the expression for the pressure (35) acquires an extra term

$$\frac{p_L}{\bar{\rho}} = \frac{H\big((H+z)\Delta U - (sU - \dot{z})L\big)^2}{(H + sL + z)^2(sL + z)} + \lambda \frac{sL^2 U\big(H\Delta U + (U + \Delta U)z + \dot{z}L\big)}{W(H + sL + z)(sL + z)}, \tag{42}$$
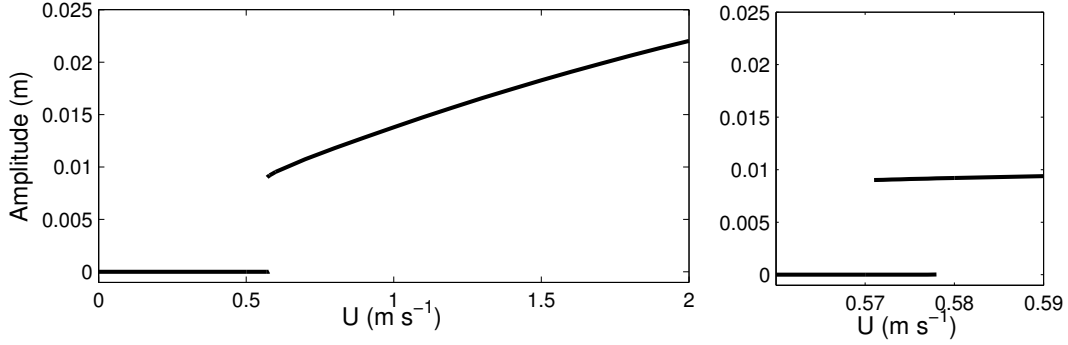
289

Figure 17: Bifurcation diagram for shallow water model showing oscillation amplitudes as a function of water speed. On the right is an enlarged view of the transition. The steady state becomes linearly unstable at around 0.578 and the upper (bouncing) branch loses stability at around 0.571. $m = 3.4$ g, $\mu = 0.2$ kg s^{-1} and $\lambda = 1$.
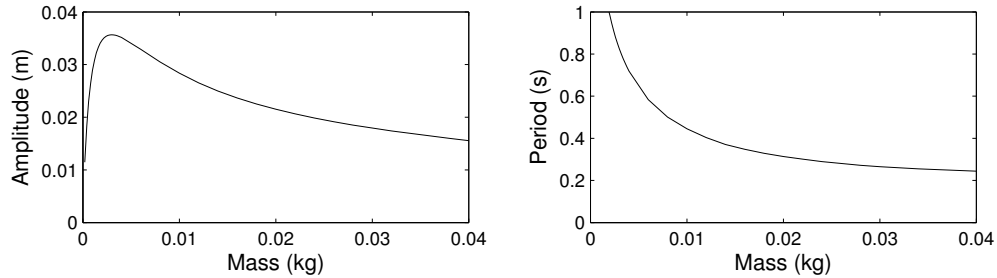

Figure 18: Amplitude and period of oscillations for the shallow water model with constant water speed $U = 1.5$ m s^{-1}, and varying mass m. $\mu = 0.2$ kg s^{-1} and $\lambda = 1$.

which also therefore appears in (36) and (37). (38) becomes

$$(sL + z)\dot{L} = -H\Delta U - (U + \Delta U)z - \dot{z}L - \lambda\frac{sL^2 U}{W}. \tag{43}$$

Including this effect reduces the size of the leading wedge of water and results in a smaller impulse from the water, so that the height of bounces is not as large. Whereas (36), (37) and (38) without the mass loss terms only have a steady state in which z is positive (the trailing edge of the paddle is *above* the undisturbed surface), including mass loss allows it to have a steady planing state which is (perhaps more reasonably) beneath the undisturbed surface. This steady state is stable at low water speeds, but becomes unstable above a threshold value, and any initial oscillations then grow until the paddle leaves the water surface. Again, the eventual oscillatory mode is independent of the initial conditions. This allows us to examine how the amplitude and period of oscillations behave as the water speed or mass vary; figure 17 shows the amplitude as the water speed is increased, and figure 18 shows how the amplitude and period vary with mass for a given speed. These should be compared qualitatively with figures 9 and 10.

The steady branch of the bifurcation diagram in figure 17 becomes linearly unstable at
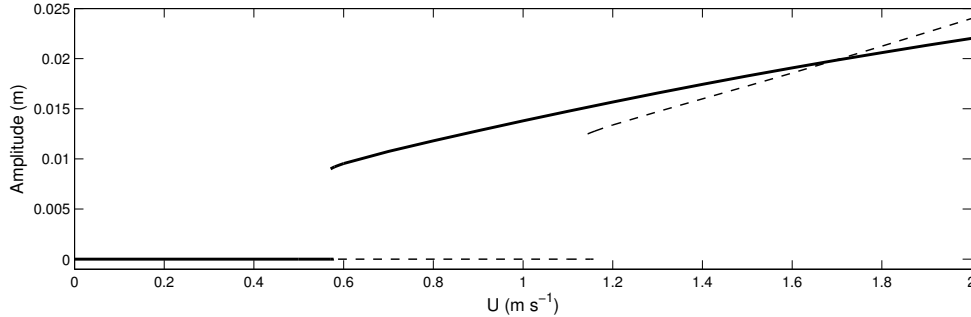
Figure 19: Bifurcation diagram for shallow water model showing oscillation amplitudes as a function of water speed for two different masses; 3.4 g (solid) and 20 g (dashed). The threshold speed for oscillations is higher for the larger mass. $\mu = 0.2$ kg s^{-1} and $\lambda = 1$.

a slightly larger water speed than where the oscillatory branch ceases to exist; this suggests the bifurcation is subcritical and there may be an unstable branch between the two. The oscillations of the upper branch are always leaving the water surface - there appear to be no steady oscillations which remain in the water. Above the threshold the amplitude increases with water speed; this is what the experiments show, except that there is no detectable jump in amplitude at which the oscillations start. The model suggests however that just below the threshold any initial oscillations will decay very slowly, so that with a small amount of noisy forcing (such as the effect of the wake in the tank), any oscillations below the threshold would be hard to get rid of. It is possible that the unavoidable roughness in the water surface might act to smooth out a sharp bifurcation in the measurements.

Figure 19 compares the bifurcation diagram for two different masses; for a larger mass the threshold velocity at which the steady state loses stability is larger, as the experiments (figure 4) suggest ought to be the case. However, it also seems that if the water speed is large enough the heavier paddle can oscillate more, thus reversing the trend seen in the experiments. It is not clear whether this is an artifact of the model or if the experiments did not reach large enough speeds to detect it.

When the paddle is really skipping and spending the majority of its time in the air, the time in the water can be viewed as a bounce, just like the bounce of an elastic ball. One way of thinking about the amplitude of the skips in this case is to consider the change in velocity (or kinetic energy) effected by each discrete bounce. Just like an elastic bounce with coefficient of normal restitution e will return an incident velocity V_{IN} at velocity $V_{OUT} = eV_{IN}$, each collision with the water will return an incident velocity V_{IN} at a different velocity which we can calculate from our model. The equilibrium amplitude which is reached is when this increase in velocity or energy is matched by the decrease due to friction during the airborne part of the motion, which we can similarly treat as providing a particular incident velocity V_{IN} (for the next collision) for any given V_{OUT}. If we plot V_{OUT} as a function of V_{IN} for the bounce and V_{IN} as a function of V_{OUT} for the ballistic motion, the steady state will be where these two curves intersect (if they do not intersect there is no steady oscillation). Provided there is one intersection, for any initial velocity we can trace a 'staircase' trajectory between the curves so that any initial condition will grow
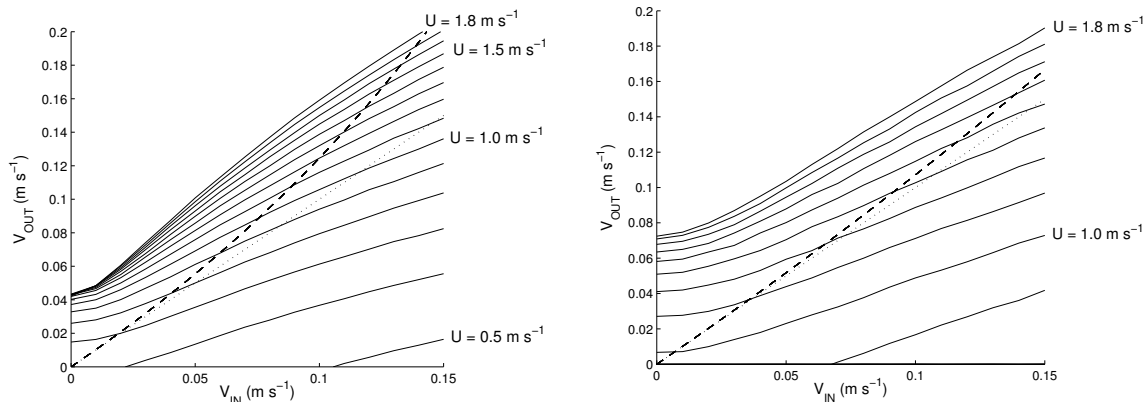
291

Figure 20: Exit velocity V_{OUT} as a function of entry velocity V_{IN} (solid lines) for collisions in the shallow water model, with $\mu = 0.1$ kg s^{-1} and $\lambda = 1$, $\alpha = 20°$, and (a) $m = 3.4$ g, (b) $m = 10$ g; The different curves correspond to different water speeds U at intervals of 0.1 m s^{-1} The dashed line shows the entry velocity as a function of exit velocity for ballistic motion with friction μ, and the dotted line is $V_{OUT} = V_{IN}$.

or decay towards the equilibrium.

Two sets of such curves are shown in figure 20 for two different masses. The collisional curves are different for different water speeds whereas the airborne curves are naturally independent of the water. For small enough U there is no intersection and therefore no steady bouncing state. As U is increased the point of intersection has larger V_{OUT}, corresponding to a larger amplitude. Unfortunately the shape of the curves depends on both U and m, and each curve has to be computed separately; there is no simple scaling which determines the intersection for different U or m.

5   A simplified shallow water model

Whilst the shallow water model presented above does a reasonable job of recreating some of the experimental trends it is not quite obvious from (36), (37) and (38) what is going on in the collision, nor how to generalise the model to deep water. If the displacement of the water surface is small, then we can attempt to extract from the equations a simpler model which includes fewer of the terms. We expect z, L and ΔU and their time derivatives all to be small in this case.

Assuming that all these terms are equally small, we find the jump conditions both become steady at leading order, and can only be satisfied if $z = 0$. We therefore expect z to be smaller than L, and the mass jump condition suggests $L^2 \sim z$. We thus look for the leading order terms in the equations when L is small and z and ΔU are quadratically small (that is, in comparison to H and U respectively; formally we treat $L/H = O(\varepsilon)$, $z/H = O(\varepsilon^2)$ and $\Delta U/U = O(\varepsilon^2)$). The equations (36), (43) and (42) become

$$-2U\Delta U - \frac{s^2 L^2 U^2}{2H^2} - \frac{U^2 z}{H} = O(\varepsilon^3), \tag{44}$$

292

$$sL\dot{L} = -H\Delta U - Uz - \lambda\frac{sL^2U}{W} + O(\varepsilon^3), \tag{45}$$

$$(M+m)\ddot{z} = -mg - \mu\dot{z} + \frac{sL^2U^2}{2H} + O(\varepsilon^3), \tag{46}$$

the first two of which simplify to

$$sL\dot{L} = -\frac{Uz}{2} + \frac{s^2L^2U}{4H} - \lambda\frac{sL^2U}{W} + O(\varepsilon^3). \tag{47}$$

It is worth considering what this approximation means in terms of the physical conservation laws on which the model is based. The leading order momentum jump condition is steady, so force balance occurs across the shock;

$$\frac{p_L}{\bar{\rho}}H_L = HU^2 - H_LU_L^2. \tag{48}$$

Moreover the u_t term in the momentum equation is smaller than the uu_x term, so that the first order pressure is determined by the steady Bernoulli equation

$$\frac{p_L}{\bar{\rho}} = \frac{1}{2}U_T^2 - \frac{1}{2}U_L^2. \tag{49}$$

The h_t term in the mass conservation equation beneath the paddle is also small, so that at leading order the mass flux beneath the paddle is uniform, $H_LU_L = H_TU_T$. The only balance which is not steady is therefore the mass balance across the shock at $x = L$ (43),

$$(H_L - H)\dot{L} = HU - H_LU_L - \lambda\frac{sL^2U}{W}. \tag{50}$$

The mass flux H_LU_L comes from combining the two momentum balances to give, up to quadratically small terms,

$$H_LU_L = U\left(\frac{2HH_LH_T^2}{H_T^2 + H_L^2}\right)^{1/2}, \tag{51}$$

but perhaps a better way of writing (50) is (correct to quadratic terms),

$$sL\dot{L} = -zU - H\Delta U - \lambda\frac{sL^2U}{W}, \tag{52}$$

in which ΔU follows from the *global* force balance

$$\frac{sF_n}{\bar{\rho}} = HU^2 - H_TU_T^2, \tag{53}$$

$$= -zU^2 - 2HU\Delta U. \tag{54}$$

The leading order force follows from integrating Bernoulli's equation for the pressure,

$$\frac{F_n}{\bar{\rho}} = \frac{sL^2U^2}{2H}, \tag{55}$$

so that combining (52) and (53), and the equation of motion, we recover (46) and (47).

The equation (52) (or (47)) for L can be thought of as mass conservation for the triangular wedge of water ahead of the paddle - the three terms on the right can be viewed respectively as the rate of mass flow into the cross sectional area of the paddle facing the fluid, the effect of the force of the paddle acting to slow down the whole water column, and the mass lost to the sides of the paddle.

5.1 Linear Stability

The simplified model (43) and (47) is in fact linear if we use the area of the water wedge $A = sL^2/2$ as a variable,

$$(M + m)\ddot{z} = -mg + \rho W \cos \alpha \frac{AU^2}{H} - \mu \dot{z}, \tag{56}$$

$$\dot{A} = -\frac{zU}{2} + \frac{sAU}{2H} - \lambda \frac{AU}{W}. \tag{57}$$

(56) is the same as our original linear equation of motion (9), except that the force now depends on the area of the leading wedge A/H rather than directly on the depth z. So we have essentially the same model, but now with a separate evolution equation for the 'wetted length' A/H.

There is a steady (planing) state

$$A_0 = \frac{mgH}{\rho W \cos \alpha \, U^2}, \qquad z_0 = -\left(\frac{2\lambda}{W} - \frac{s}{H}\right) \frac{mgH}{\rho W \cos \alpha \, U^2}, \tag{58}$$

and we can examine its stability by writing the equations in the matrix form

$$\begin{pmatrix} \dot{A} \\ \dot{z} \\ \ddot{z} \end{pmatrix} = \begin{pmatrix} b & -a & 0 \\ 0 & 0 & 1 \\ c & 0 & -d \end{pmatrix} \begin{pmatrix} A - A_0 \\ z - z_0 \\ \dot{z} \end{pmatrix}, \tag{59}$$

where

$$a = \frac{U}{2}, \qquad b = \frac{sU}{2H} - \frac{\lambda U}{W}, \qquad c = \frac{\rho W \cos \alpha}{M + m} \frac{U^2}{H}, \qquad d = \frac{\mu}{M + m}. \tag{60}$$

Solutions of the form $e^{\lambda t}$ exist provided λ satisfies

$$\lambda^3 - (b - d)\lambda^2 - bd\lambda + ac = 0. \tag{61}$$

Since a and c are positive this clearly has one negative real root λ_0 and two other roots which could be real (in which case they are positive) or complex, but whose real part is of interest. If we write the complex roots as $\beta \pm i\alpha$ then

$$0 = (\lambda - \lambda_0)(\lambda - \beta - i\alpha)(\lambda - \beta + i\alpha) = \lambda^3 - (\lambda_0 + 2\beta)\lambda^2 + (\beta^2 + \alpha^2 + 2\beta\lambda_0)\lambda - (\beta^2 + \alpha^2)\lambda_0, \tag{62}$$

from which we require

$$\lambda_0 + 2\beta = b - d, \quad \beta^2 + \alpha^2 + 2\beta\lambda_0 = -bd, \quad (\beta^2 + \alpha^2)\lambda_0 = -ac. \tag{63}$$

If b is positive, the coefficient of λ^2 implies β must be positive (so the steady state is unstable), but if b is sufficiently negative we could have negative β (and therefore stability). The threshold for stability is (setting $\beta = 0$)

$$d > \frac{b}{2} + \left(\frac{b^2}{4} - \frac{ac}{b}\right)^{1/2}, \tag{64}$$
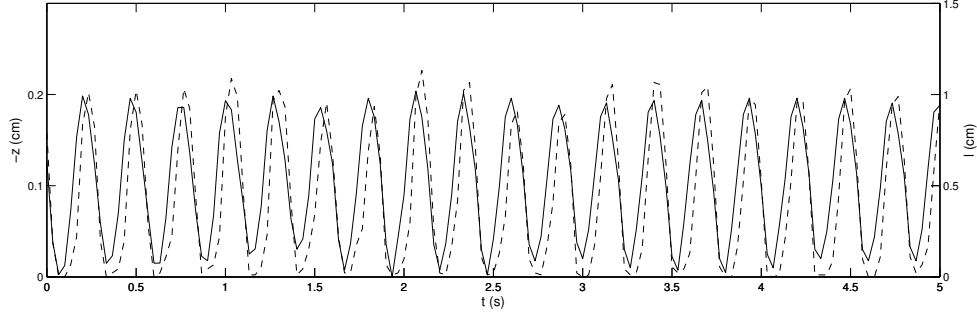
Figure 21: Time series of vertical position of paddle z (solid, left axis, larger values of $-z$ are deeper in the water), and wetted length of the paddle l (dashed, right axis). These are from measurements every 1/30 of a second.

or in terms of the parameters

$$\frac{\mu}{M+m} > \frac{U}{2}\left(\frac{s}{2H} - \frac{\lambda}{W}\right) + \frac{U}{2}\left(\left(\frac{s}{2H} - \frac{\lambda}{W}\right)^2 - \frac{2\rho W \cos\alpha}{(M+m)H\left(\frac{s}{2H} - \frac{\lambda}{W}\right)}\right)^{1/2}. \quad (65)$$

Thus there is a critical level of friction needed in order to stabilise the system in the planing state, and the critical value increases linearly with the speed of the water U. If there is not sufficient friction the steady state will be unstable and perturbations will grow exponentially until they reach the surface (that is, once A reaches 0). The hydrodynamic force then switches off, and this non-linearity serves to set the amplitude of the bounces.

5.2 A shallow water experiment

As a qualitative test of the shallow water model, including the idealization of the splash up as a shock, we designed an alternative experiment which comprised water flow under gravity down an inclined plane. The flow was maintained by pumping water from a lower tank into an upper one which overflowed down the ramp into the lower one. The flow on the ramp was about 4 mm deep and travelling at about 60 cm s^{-1}. The same paddle was placed in this stream and, when light enough, was observed to oscillate up and down, coming clear of the water momentarily. The paddle was widened so as to take up the full width of the stream and minimise the flow around the sides. This made the oscillations greater, as the theory would suggest. When the paddle was heavy enough there was a steady state in which a large (several cm) wedge of fluid built up ahead, whereas when the paddle was light enough this wedge of fluid oscillated to and from the trailing edge.

The crucial factor in the model we have proposed is the fact that the wetted length (or equivalently in this case, the size of the leading wedge of water) does not respond instantaneously to the depth of the paddle in the water. The lag between changing the depth and increasing the wetted length is the essential mechanism in driving the oscillations.

By recording the position of the front of the leading wedge of water at the same time as the vertical position of the paddle we are able to verify this lag experimentally. Figure
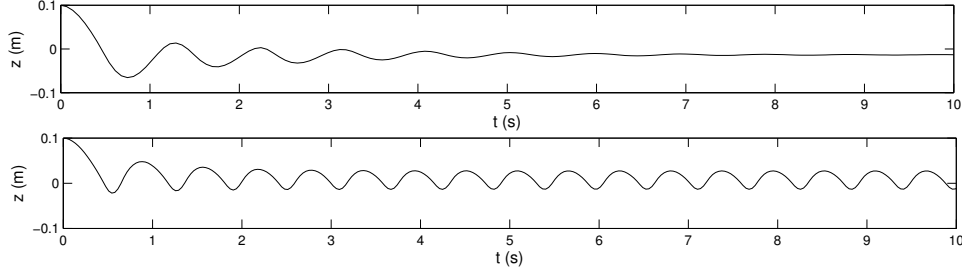
295

Figure 22: Paddle trajectories for the generalized deep water model (66) and (67), released from rest at 10 cm height, with water speed (a) 0.5 m s^{-1} (below threshold) and (b) 1 m s^{-1} (above threshold). $m = 10$ g, $\mu = 0.2 \text{ kg s}^{-1}$ and $\lambda = 4$.

21 shows the position of the wetted front L and the depth of the paddle $-z$, and there is a clear lag between the two.

This experimental setup worked well and it would be good to conduct more tests with the same setup, particularly with a larger flow rate so that the speed of the water can be varied and its effect carefully monitored. A more precise bifurcation diagram might be found in this way than we were able to do in the rotating tank.

5.3 Generalization to deeper water

We now attempt to use the simplified model of the previous section to generalize to deeper water. (56) and (57) both contain the expression for the force $F_n = AU^2/H$ and this is the only place in which the water depth H appears. It seems natural to suppose that the water depth in this context represents the depth over which the presence of the paddle affects the water; for shallow water this is the whole depth, but for deeper water it might be expected to be on the scale of the horizontal perturbation (consider an analogy with surface gravity waves, when the phase speed changes from $(gH)^{1/2}$ to $(g/k)^{1/2}$ where k is the horizontal wave number). We therefore consider it appropriate to replace H in (56) and (57) by L,

$$(M + m)\ddot{z} = -mg + \rho W \cos \alpha \, \frac{sLU^2}{2} - \mu \dot{z}, \tag{66}$$

$$sL\dot{L} = -\frac{zU}{2} + \frac{s^2 UL}{4} - \lambda \frac{sL^2 U}{2W}. \tag{67}$$

The steady state is now

$$L_0 = \frac{2mg}{\rho W \cos \alpha \, sU^2}, \qquad z_0 = -\frac{mg}{\rho W \cos \alpha \, U} \left(\frac{2\lambda mg}{s\rho W^2 \cos \alpha \, U^2} - \frac{s}{2} \right). \tag{68}$$

Linearised perturbations about this again satisfy

$$\begin{pmatrix} \dot{L} \\ \dot{z} \\ \ddot{z} \end{pmatrix} = \begin{pmatrix} b & -a & 0 \\ 0 & 0 & 1 \\ c & 0 & -d \end{pmatrix} \begin{pmatrix} L - L_0 \\ z - z_0 \\ \dot{z} \end{pmatrix}, \tag{69}$$
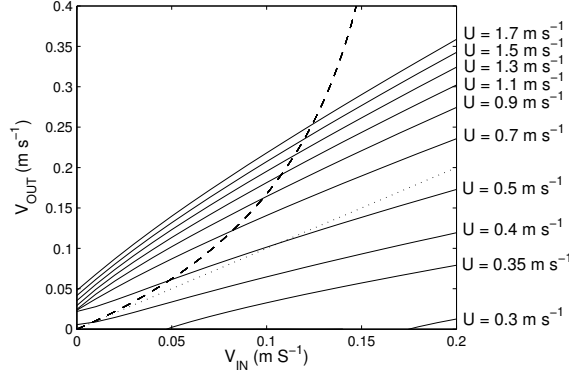
296

Figure 23: Exit velocity V_{OUT} as a function of entry velocity V_{IN} (solid) for deep water model (66) and (67) This is for a mass of 3.4 g and paddle of width 7 cm with mass loss $\lambda = 1$ and friction $\mu = 0.2$ kg s^{-1}. The different curves correspond to different water speeds as labelled. The dashed line shows V_{IN} as a function of V_{OUT} as determined by resistance in the ballistic motion and the dotted line is the line $V_{IN} = V_{OUT}$.

but now with

$$a = \frac{\rho W \cos \alpha \ U^3}{4mg}, \qquad b = \frac{\rho W \cos \alpha \ s^2 U^3}{8mg} - \frac{\lambda U}{W}, \qquad c = \frac{\rho W \cos \alpha s U^2}{2(M+m)}, \qquad d = \frac{\mu}{M+m}. \tag{70}$$

The stability criterion is as in (64); b must be negative, and

$$\frac{\mu}{M+m} > \frac{\rho W \cos \alpha \ s^2 U^3}{16mg} - \frac{\lambda U}{2W}$$

$$+ \frac{1}{2} \left(\left(\frac{\rho W \cos \alpha \ s^2 U^3}{8mg} - \frac{\lambda U}{W} \right)^2 - \frac{\rho^2 W^2 \cos^2 \alpha \ s U^5}{2mg(M+m) \left(\frac{\rho W \cos \alpha \ s^2 U^3}{8mg} - \frac{\lambda U}{W} \right)} \right)^{1/2}. \tag{71}$$

Again we find the steady state is stable provided there is sufficient friction, and the critical level of friction increases with water speed. Above this, perturbations grow until they reach the water surface, and they then settle into a natural amplitude of bouncing. This amplitude is independent of the initial conditions - and the amplitude is larger for larger water speeds. Figure 22 shows example trajectories for U smaller than and larger than the threshold speed for instability, when the paddle is dropped into the water from a height. The same steady oscillations would be reached in the latter case if the paddle were initially perturbed slightly from the steady planing state.

6   Wagner model: potential flow

The previous sections have identified the rise of water ahead of the paddle, and the time lag necessary for this to happen, as a mechanism for generating super-elastic bounces from the water surface. We have attempted to model this in a shallow water setting and with an
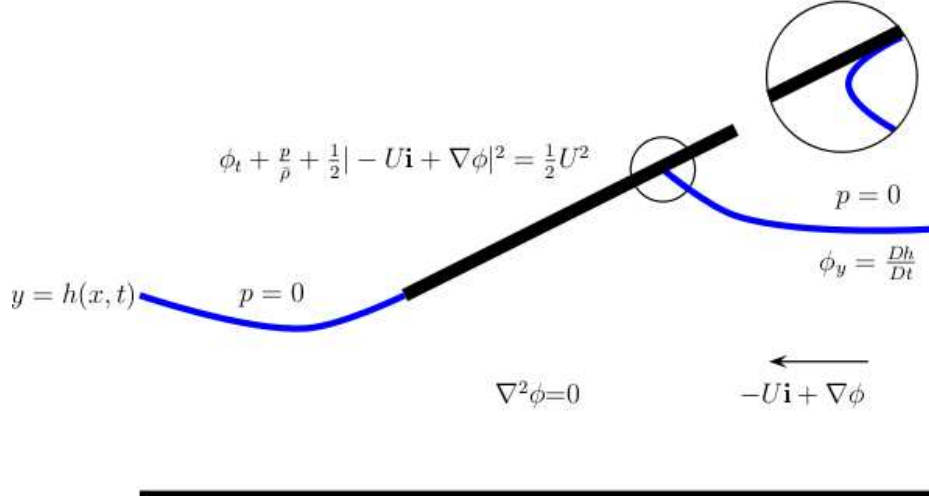
Figure 24: Potential flow problem for a paddle impacting the free surface of an inviscid irrotational fluid, moving at undisturbed speed U. The free surface is at atmospheric pressure $p = 0$, as well as being subject to a kinematic condition. The kinematic condition also holds on the paddle, and the pressure there determines the vertical force on the paddle, which can be used to determine how the paddle moves.

ad-hoc generalisation to deeper water. Both of these essentially use parameterisations for the effect of the paddle on the water flow.

A different approach is to attempt to calculate the water flow due to the paddle explicitly. This is again easiest in two dimensions, where we assume the flow is irrotational. We can then write the velocity as $\mathbf{u} = -U\mathbf{i} + \nabla\phi$, where ϕ is the disturbance potential satisfying Laplace's equation. We assume the stream occupies the space $-H < y < 0$, and consider the situation shown in figure 24. This type of problem has been reasonably well established as a so-called Wagner problem [20, 7, 5, 6].

The pressure is given by Bernoulli's equation, neglecting gravity,

$$\bar{\rho}\phi_t + p + \frac{1}{2}\bar{\rho}| - U\mathbf{i} + \nabla\phi|^2 = \frac{1}{2}\bar{\rho}U^2, \tag{72}$$

the constant being determined by a steady uniform upstream condition, and zero atmospheric pressure. The free surface $y = h(x, t)$ has kinematic condition $\phi_y = Dh/Dt$, and the pressure there must be atmospheric.

If a paddle enters the water, suppose it occupies the region of the surface $0 < x < L(t)$. L here is treated as the 'turnover' point (figure 24); there will be a small jet of water ejected ahead of the paddle, but the appreciable force comes only from the wetted region up to the turnover point L. For the purposes of this problem we disregard the details of this region and the high speed jet entirely; see [7] for further discussion. For this wetted part of the surface the relevant boundary condition is that the normal velocity of the water must equal the normal velocity of the paddle. If the paddle is a flat plate moving in a vertical plane with angle of attack α, then the normal is $\mathbf{n} = (-\sin\alpha, \cos\alpha)$, so that

$$-(-U + \phi_x)\sin\alpha + \phi_y\cos\alpha = \dot{z}\cos\alpha, \tag{73}$$

298

$$\phi_y = h_t - Uh_x \qquad\qquad \begin{array}{c} h = z + sx \\ p = -\phi_t + U\phi_x \\ \phi_y + s(U - \phi_x) = \dot{z} \end{array} \qquad\qquad \phi_y = h_t - Uh_a$$
$$\phi_t - U\phi_x \qquad\qquad\qquad\qquad\qquad\qquad\qquad \phi_t - U\phi_x$$

$$x = 0 \qquad\qquad\qquad\qquad x = L(t)$$
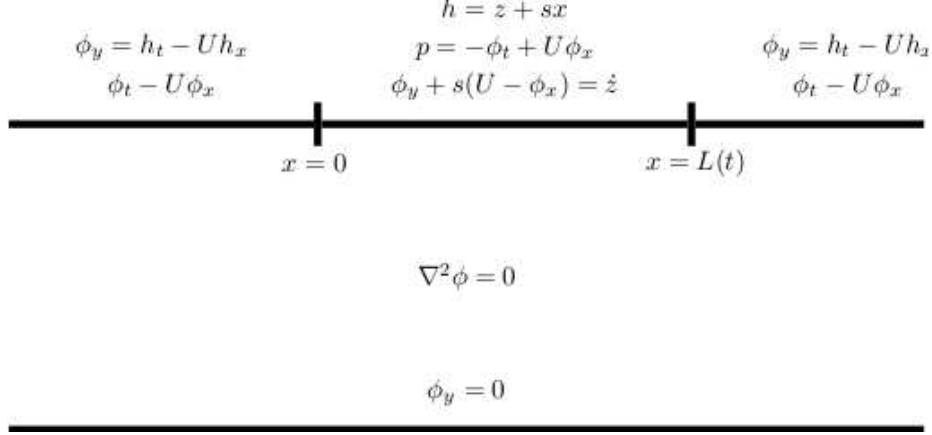
$$\nabla^2\phi = 0$$

$$\phi_y = 0$$

Figure 25: The linearised Wagner problem for a bouncing paddle $h_p = z + sx$ occupying the region $0 < x < L(t)$ of the surface of an inviscid irrotational fluid. The boundary conditions are as in figure 24, but are now applied at the undisturbed surface $y = 0$.

where $\dot{z}$ is the vertical velocity of the paddle. We also know the height of the paddle

$$h_p(x, t) = z + x \tan \alpha, \tag{74}$$

where z is the vertical position of the trailing edge above the undisturbed surface $y = 0$. The unknown position of the leading edge $x = L(t)$ is determined by the condition that the free surface height here is equal to the height of the paddle:

$$h(L(t), t) = h_p(L(t), t). \tag{75}$$

If we consider the linearised form of this problem (figure 25) we have

$$\nabla^2\phi = 0, \quad -H < y < 0; \qquad \phi_y = 0 \quad \text{at} \quad y = -H; \qquad \phi_x \to 0 \quad \text{as} \quad x \to \pm\infty, \tag{76}$$

At the surface $y = 0$,

$$\left.\begin{array}{l} \phi_y = h_t - Uh_x, \\ 0 = -\phi_t + U\phi_x, \end{array}\right\} \quad \text{for} \quad x < 0, \quad x > L(t), \tag{77}$$

$$\left.\begin{array}{l} h = h_p = z + sx, \\ \phi_y - s\phi_x = \dot{z} - sU, \end{array}\right\} \quad \text{for} \quad 0 < x < L(t), \tag{78}$$

where $s = \tan \alpha$ is the slope of the paddle. At $x = L(t)$,

$$h(L(t), t) = h_p(L(t), t). \tag{79}$$

For a given $z(t)$ these provide the equations and boundary conditions to be solved for $\phi(x, y, t)$ and $h(x, t)$. However this is coupled to the equation of motion for the paddle,

$$(M + m)\ddot{z} = -mg + F_n \cos \alpha - \mu\dot{z} \tag{80}$$

since the normal force F_n is

$$F_n = \int_0^{L(t)} p \ \mathrm{d}x = \bar{\rho} \int_0^{L(t)} -\phi_t + U\phi_x \ \mathrm{d}x. \tag{81}$$

We can attempt to solve this problem numerically by solving Laplace's equation for ϕ at every time step using the pressure boundary conditions for $x < 0$ and $x > L$ and the kinematic boundary condition for $0 < x < L$ (the other boundary conditions are $\phi_y = 0$ at the bottom and $\phi_x = 0$ at the sides, which we try to make far away from the paddle). Then the kinematic boundary conditions on $x < 0$ and $x > L$ give the motion of the boundary there (with boundary condition $h = 0$ at $x = +\infty$), whilst Bernoulli's equation for $0 < x < L$ gives the pressure there and hence the acceleration of the paddle. We can therefore find the new position of the paddle and the free surface and find the new value of L at which these surfaces are equal. This gives the region over which the different boundary conditions should be applied for Laplace's equation at the next time step.

The solutions indicate that if the background stream flow U is large enough the paddle can receive a super-elastic kick from the water, just as we found in the shallow water model. In this case any initial condition will reach a steady bouncing state, with the amplitude dependent on the water speed and paddle mass. The water ahead of the paddle rises up to meet it, and the paddle does not leave the water until it is some distance above the undisturbed level at which it entered it. At slower speeds there seems to be a steady planing state in which the pressure balances the weight of the paddle.

It seems therefore that although the quantitative values (the amplitudes of the bounces and the speed at which bouncing starts) are different, the same instability mechanism is inherent in this model as in the shallow water model. This is reassuring since the potential flow captures more of the fluid dynamics than the shallow water assumptions do, but given the computational intensity, this model is not particularly useful nor wholly satisfying for understanding what is going on.

7   Conclusion

A light paddle towed along the surface of flat water will continually bounce, or skip, along provided it is pulled fast enough. The experiments we conducted (in which the paddle could move vertically and the water flowed past) suggest that for a given paddle mass there is a threshold water speed below which it planes steadily through the water and above which it oscillates up and down, leaving the surface and skipping if the oscillations are large enough. The amplitude of oscillations increases with the water speed above the threshold. For a given water speed there seems to be a natural bouncing mode (with characteristic amplitude and period) to which any initial condition evolves.

The threshold velocity at which skipping starts is larger for a heavier paddle and lower for a wider paddle, and for a given velocity lighter and wider paddles tent to bounce higher. When bouncing occurs the collision with the water appears to be super-elastic; the paddle gains energy from the water.

We have described several models to try to explain the experimental findings; the key mechanism we identify which causes the instability is the *transient* response of the water to

the paddle moving in and out. The most simple models which treat the water's response as a steady function of paddle displacement cannot explain the skipping. Instead, the variation of the 'wetted length' over the collision must be explicitly accounted for.

A shallow water description, in which the splashed up water ahead of the paddle is treated as a shock, indicates that there should be a bifurcation at a critical water speed above which the steady planing state becomes unstable and a bouncing mode, with super-elastic bounces, is reached. The amplitude of oscillations is larger for larger water speed and wider paddle, as found in the experiments.

A simplification and generalization to deeper water allow for a simple two o.d.e. description of the system which again has the bifurcation and correct dependence on the various parameters. The model is not quantitatively comparable to the experiment but this may be due to uncertainties in the parameterized effects of the water flow beneath and around the paddle.

A two dimensional linearized potential flow model verifies that accounting for the time evolution of the wetted length can allow super-elastic bounces and destabilize the steady planing state.

The shallow water model motivated a further experiment in which the paddle was placed in a shallow stream. We were able to verify the lag between vertical paddle position and wetted length during oscillations. This setup worked well and it would be worthwhile to do some further studies with varying the flow speed. The setup was more robust, easier to use, and avoids the complications of the wake in the rotating tank. With more careful measurements we might also be able to test more critically the models suggested here.

8   Acknowledgements

References

[1] B. J. BINDER AND J.-M. VANDEN-BROECK, *Free surface flows past surfboards and sluice gates*, Euor. J. App. Math., 16 (2005), pp. 601–619.

[2] L. BOCQUET, *The physics of stone skipping*, Am. J. Phys., 71 (2003), pp. 150–155.

[3] C. CLANET, F. HERSEN, AND L. BOCQUET, *Secrets of successful stone-skipping*, Nature, 427 (2004).

[4] A. E. GREEN, *The gliding of a plate on a stream of finite depth*, Proc. Camb. Philos. Soc., 31 (1935), pp. 589–603.

[5] S. D. HOWISON, J. R. OCKENDON, AND J. M. OLIVER, *Deep- and shallow-water slamming at small and zero deadrise angles*, J. Eng. Math., 42 (2002), pp. 373–388.

[6] ——, *Oblique slamming, planing and skimming*, J. Eng. Math., 48 (2004), pp. 321–337.

[7] S. D. Howison, J. R. Ockendon, and S. K. Wilson, *Incompressible water-entry problems at small deadrise angles*, J. Fluid. Mech., 222 (1991), pp. 215–230.

[8] W. Johnson, *The richochet of spinning and non-spinning spherical projectiles, mainly from water. Part II: An outline of theory and warlike applications*, Int. J. Impact Engng., 21 (1998), pp. 25–34.

[9] A. Korobkin, *Shallow-water impact problems*, J. Eng. Math., 35 (1999), pp. 233–250.

[10] H. Kuninaka and H. Hayakawa, *Anomalous behavior of the coefficient of normal restitution in oblique impact*, Phys. Rev. Lett., 93 (2004).

[11] M. Y. Louge and M. E. Adams, *Anomalous behavior of normal kinematic restitution in the oblique impacts of hard sphere on an elastoplastic plate*, Phys. Rev. E, 65 (2002).

[12] P. R. Payne, *The water rise in front of a model planing hull*, Experiments in Fluids, 17 (1994), pp. 96–104.

[13] L. Rosellini, F. Hersen, C. Clanet, and L. Bocquet, *Skipping stones*, J. Fluid. Mech., 543 (2005), pp. 137–146.

[14] T. Sugimoto, *Mechanics of the surf skimmer revisited*, Am. J. Phys., 71 (2003), pp. 144–149.

[15] N. Taberlet, S. W. Morris, and J. N. McElwaine, *Washboard road: The dynamics of granular ripples formed by rolling wheels*, Phys. Rev. Lett., 99 (2007).

[16] L. Ting and J. B. Keller, *Planing of a flat plate at high Froude number*, Phys. Fluids., 17 (1974), pp. 1080–1086.

[17] E. O. Tuck and A. Dixon, *Surf-skimmer planing hydrodynamics*, J. Fluid. Mech., 205 (1989), pp. 581–592.

[18] J.-M. Vanden-Broeck, *Numerical calculations of the free-surface flow under a sluice gate*, J. Fluid. Mech., 330 (1997), pp. 339–347.

[19] T. Von Karman, *The impact of sea planes during landing.*, NACA Tech. Note 321, (1929).

[20] H. Wagner, *Über Stoß- und gleitvorgänge an der Oberflaäche von Flüssigkeiten (Phenomena associated with impacts and sliding on liquid surfaces)*, Zeitschr. Angew. Math. Mech., 12 (1932), pp. 193–215.